Int. J. Nano Dimens., 7(1): 15-24, Winter 2016
DOI: 10.7508/ijnd.2016.01.002

Research Paper

Synthesis, characterization and optical band gap of Lithium cathode materials: $Li_2Ni_8O_{10}$ and $LiMn_2O_4$ nanoparticles

J. Nouri [1]; T. Khoshravesh [1]; S. Khanahmadzadeh [1]; A. Salehabadi [2]; M. Enhessari [, 2]*

[1]Department of Chemistry, Mahabad Branch, Islamic Azad University, Mahabad, Iran
[2]Department of Chemistry, Naragh Branch ,Islamic Azad University, Naragh, Iran

Received 08 May 2015; revised 01 September 2015; accepted 20 September 2015; available online 14 October 2015

ABSTRACT: $Li_2Ni_8O_{10}$ and $LiMn_2O_4$ Nanoparticles as cathode materials for lithium ion battery were successfully synthesized using lithium acetate, nickel and manganese acetate as Li, Ni and Mn sources and stearic acid as a complexing reagent. The structure of the obtained products was characterized by FT-IR and XRD. The shape, size and distribution of the $Li_2Ni_8O_{10}$ and $LiMn_2O_4$ nanoparticles were observed by SEM. Optical band gap and magnetic properties were determined by diffuse reflectance spectroscopy (DRS) and vibrating sample magnetometer (VSM). $Li_2Ni_8O_{10}$ and $LiMn_2O_4$ spinels were identified as the main crystalline phases. The particles size of both, $Li_2Ni_8O_{10}$ and $LiMn_2O_4$ nanoparticles is around 24 to 32 nm. Optical band gap of $Li_2Ni_8O_{10}$ and $LiMn_2O_4$ are 1.40 eV and 1.16 eV, respectively. Therefore, lithium nickel and lithium manganese oxide nanoparticles can be used as semiconductor materials in electrical devices. VSM curve showed paramagnetic behavior of $LiMn_2O_4$ nanoparticles. Moreover, color parameters were obtained by colorimetric analysis of $LiMn_2O_4$ indicating characteristic values of L*=25.820, a*=1.607 and b*= -1.143.

Keywords: *$Li_2Ni_8O_{10}$; $LiMn_2O_4$; Nanoparticles; Optical band gap; Semiconductor.*

INTRODUCTION

The spinel $Li_2Ni_8O_{10}$ and $LiMn_2O_4$ are two promising cathode materials with economical and environmental advantages as compared with layered compounds such as $LiCoO_2$ and $LiNiO_2$ [1]. Reasonable price and environmental concerns are two main advantages of the as prepared nano-catalysts. In general, Solid-state reaction [2-4], hydrothermal method [5, 6], combustion synthesis [7-9], sol-gel [10], co-precipitation [11], melt-impregnation [12], the citric acid gel method [13, 14], the tartaric acid gel method [15, 16], and Pechini process [17] have been developed to synthesize the multi-metal catalysts. Among them, the solid-state reaction and combustion synthesis methods have been achieved more attention as; they show superior performance in producing high quality cathode materials. But the former needs high temperature and long heating period. Ahn *et al.* [18] have reported the synthesis of spinel $LiMn_2O_4$ by solid-state reaction. The $LiMn_2O_4$ powder was obtained in their study by calcining at 750 °C for 48 h. Yang *et al.*, [19] have reported the synthesis of spinel $LiMn_2O_4$ by combustion process. The spinel $LiMn_2O_4$ in their study has been obtained by the combustion reaction following further calcining in 800°C for 24h. Here, production of the catalysts by combustion method is difficult due to the fast reaction rate, therefore, high quality cathode materials need further calcining in high temperature and long time. To overcome these deficiencies, it is highly recommended to develop a simple and rapid method. Obviously, the preparation of spinel $LiMn_2O_4$ phase by solid-state reactions involves the raw materials of manganese oxides, nitrate or carbonate with lithium hydroxide, nitrate or carbonate at temperatures 700-900°C, and the final product usually contains the impurity phases, irregular morphology, larger particle size, and broader particle size distribution [20, 21]. In general, single-phase, homogeneity, uniform particle morphology, and large surface area are considered as desirable characteristics in solar electrodes batteries.

In current study, stearic acid gel method was

*Corresponding Author: Morteza Enhesari
Email: *enhessari@gmail.com*
Tel.: (+98) 9126592998
Fax: (+98) 8644463920

performed to synthesize both $Li_2Ni_8O_{10}$ and $LiMn_2O_4$ nanoparticles, directly from the starting materials. For precursor preparation, diffusion of metallic cations from aqueous to organic phase was occured [22]. Finally, the properties of as prepared nanoparticles were analyzed.

EXPERIMENTAL

Material

The as mention source materials were dissolved in de-ionized water, the molar ratio of the metal ions Li^+:Ni^{2+} and Li^+:Mn^{2+} controlled in the ratio of 1:4 and 1:2, respectively. The metal–ion solutions were mixed with the melted stearic acid. During mixing, the solution was transformed into a viscous gel. The gel was subsequently heated in an oven at 100 °C to remove the moisture. After drying, both, the lithium nickel acetate and lithium manganese acetate precursors were agglomerated [23]. The precursor was then heated at 200 to 350°C for 72 hours to slowly remove the unwanted materials. Subsequently, the calcination process was conducted at 800 °C for 4 hours in air. Finally, the calcined nanoparticles were furnace-cooled down to room temperature for further investigation. The schematic representation of as mention procedure is shown in Fig.1.

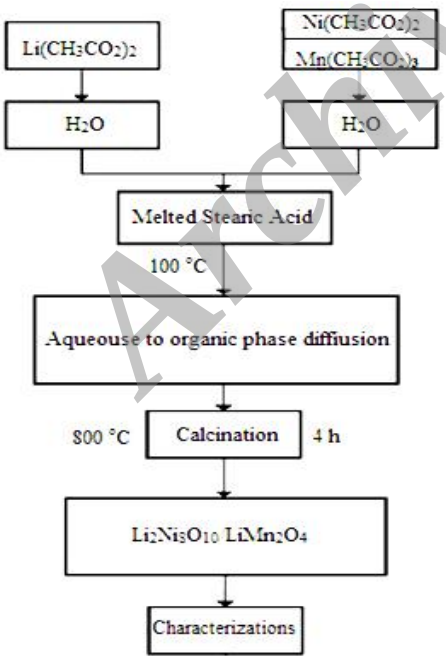

Fig.1: Schematic representation of nanoparticles ($Li_2Ni_8O_{10}$ and $LiMn_2O_4$) synthesis method.

Characterizations

Spectroscopic analysis was carried out using FTIR Perkin-Elmer spectrometer RX1 to study the structure coordination of the precursors. Each sample was mixed with KBr and examined at the wave number range from 400 to 4000 cm^{-1}. The phase identity, crystal structure, and lattice constants of the materials were investigated using Rigaku X-ray diffractometer (XRD, PTS 3003) with the Cu Kα radiation at 30 kV, 20 mA. The XRD data were collected between 15 and 80° of 2θ angles. Lattice constants were determined by a least-squares refinement of the d-spacing, which were measured in comparison with an internal standard of pure Ag. The morphology and size distribution of the nanoparticles were measured using scanning electron microscopy (SEM, KYKY-EM3200-UK).

The magnetic properties of $LiMn_2O_4$ nanoparticles calcined at 800 °C carried out by Vibrating Sample Magnetometer (VSM, BHV-55, Riken, Japan). The optical band gap of the nanoparticles carried out by Diffuse Reflectance Spectroscopy (DRS, SCINCO S4100). The color parameters ($L^*.a^*.b^*$) of $LiMn_2O_4$ nanoparticles calcined at 800 °C identified by Reflectance Spectrophotometer (RS, Ihara-spcam spectrophotometer).

RESULTS AND DISCUSSION

FTIR study

The FTIR spectra of $Li_2Ni_8O_{10}$ and $LiMn_2O_4$ nanoparticles are shown in Fig. 2. The $Li_2Ni_8O_{10}$ and $LiMn_2O_4$ nanoparticles show a number of vibration frequencies below 1000 cm^{-1}.These absorption bands confirm metal-oxygen *i.e.* Li-O, Ni-O and Mn-O vibration frequencies [24]. The peak at around 418 cm^{-1} in both $Li_2Ni_8O_{10}$ and $LiMn_2O_4$ spectra indicate the metal-metal (Li-Ni & Li-Mn) vibration frequency [25]. Moreover, two bands at 502 and 616 cm^{-1} are attributed to the asymmetric stretching modes of MnO_6 group.

Structural analysis

Fig. 3 shows the X-ray diffraction pattern of synthesized $Li_2Ni_8O_{10}$ and $LiMn_2O_4$ nanoparticles. The presence of sharp bands (Indexed in the pattern) in the XRD patterns of metal oxides either $Li_2Ni_8O_{10}$ or $LiMn_2O_4$ are supported by literature (JCPDS 23-0362 and 35-782) with the presence of minor Ni-O and Mn_3O_4. Hexagonal crystal structure of $Li_2Ni_8O_{10}$ can be confirmed by a series of sharp peaks at 2 θ equal to 18.94º (003), 38.15º (102), 44.29º (104) and 64.25º (110).

Moreover, a hexagonal impurity appears to exist over a wide range of Lithium concentration. The spinel structure of $LiMn_2O_4$ with space group Fd3m 6 lithium ions occupy the tetrahedral sites and the doped metal ions reside at the octahedral sites 6 can be clearly identified according to (111), (311), (400), and (440) Miller index parameters. The nanoparticles diameter was calculated from the XRD pattern according to the line width of the (311) plane reflection peak using the following Scherrer equation (1),

$$D = \frac{k\lambda}{\beta \cos \theta} \quad (1)$$

where θ is the angle, λ is the wavelength (0.15418 nm), β is the width of the XRD peak at half height and k is a shape factor, about 0.9 for spherical shaped nanoparticles. The particle size calculated from the equation was about 22 nm in the case of $LiMn_2O_4$ and about 30 nm for $Li_2Ni_8O_{10}$. The results are obviously supported by SEM observations.

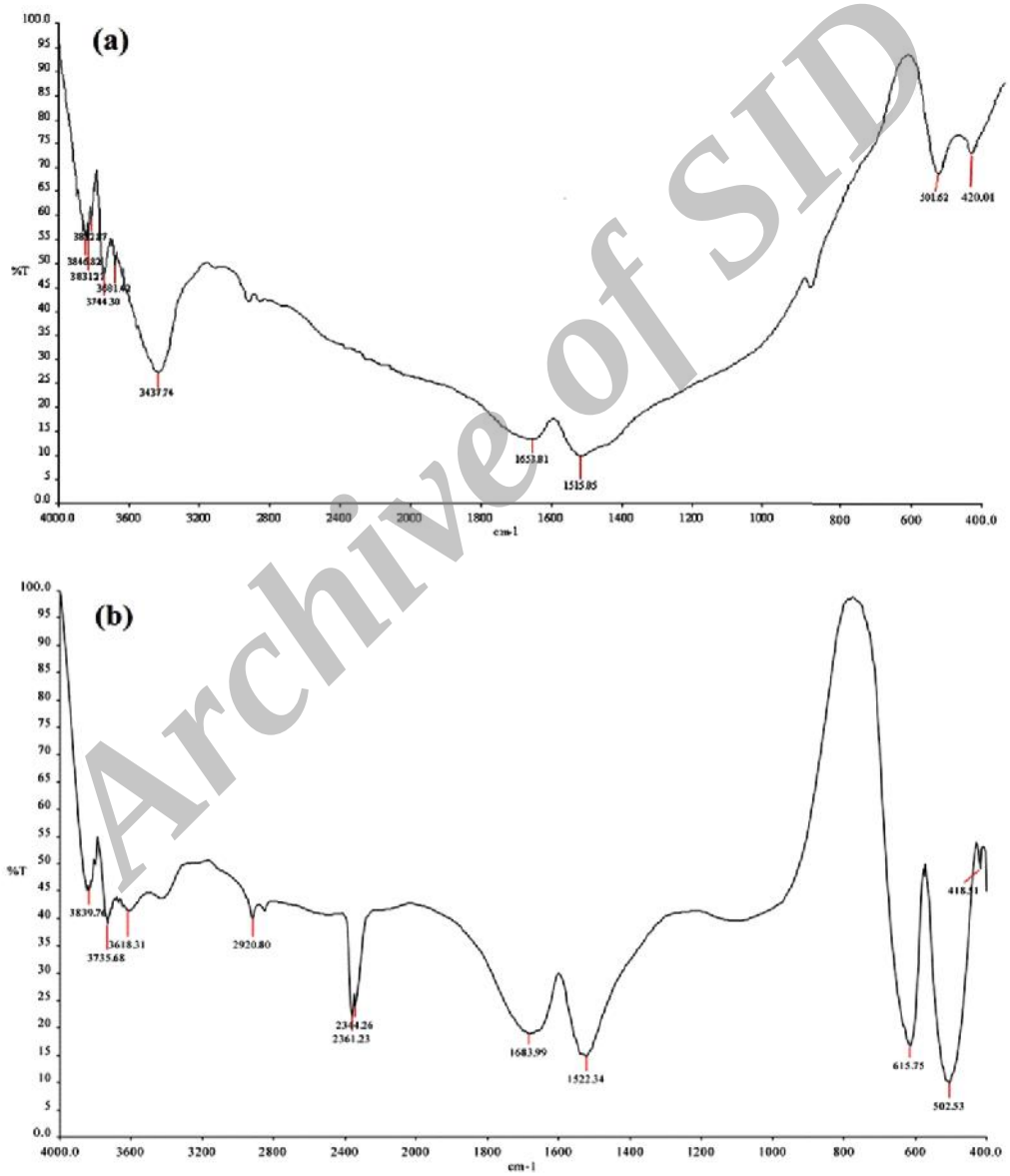

Fig. 2: FTIR spectra of (a) $Li_2Ni_8O_{10}$ and (b) $LiMn_2O_4$ nanoparticles.

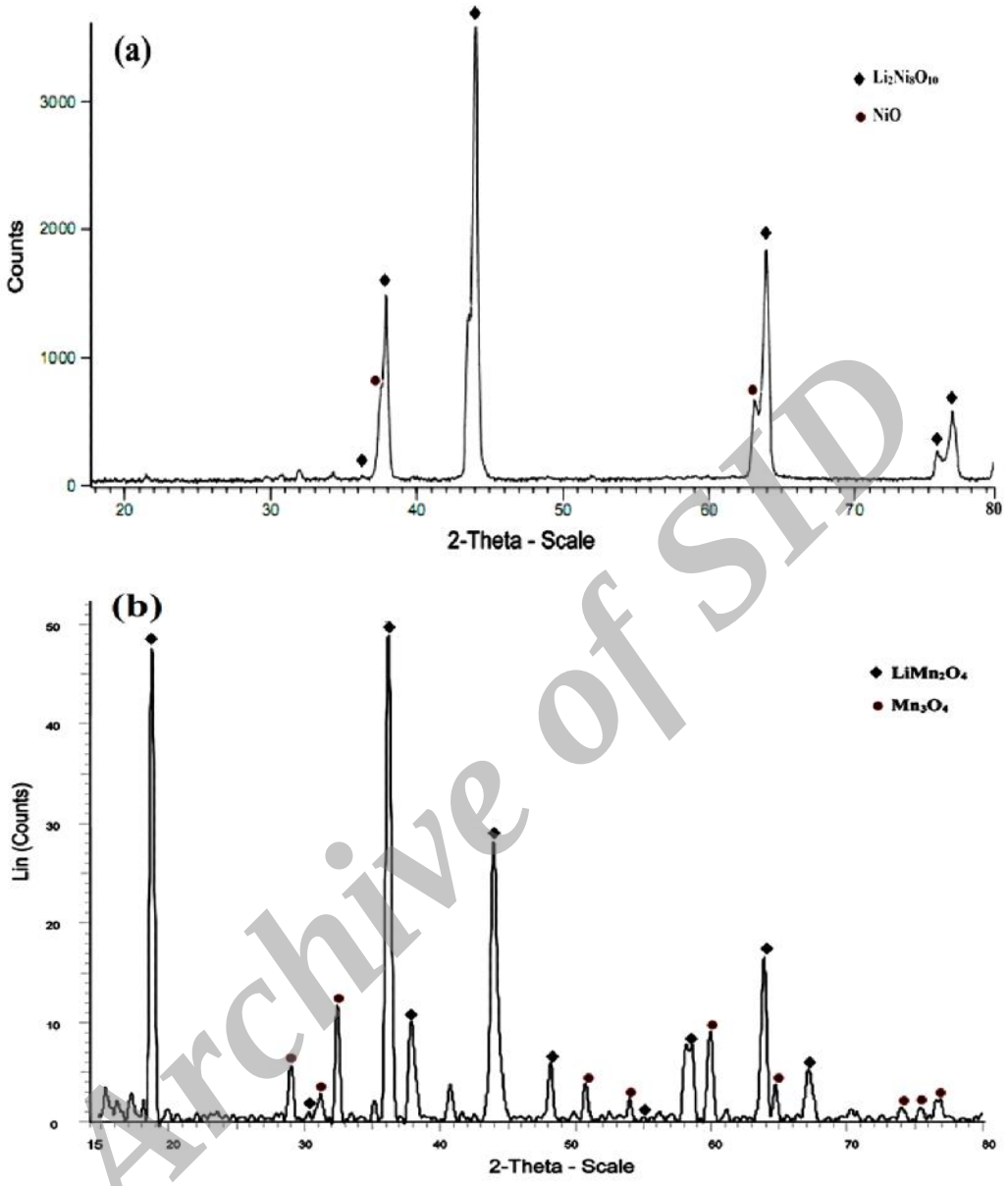

Fig. 3: XRD patterns of (a) $Li_2Ni_8O_{10}$ and (b) $LiMn_2O_4$ nanoparticles.

Morphology

The surface morphologies of $Li_2Ni_8O_{10}$ and $LiMn_2O_4$ nanoparticles are shown in Fig. 4. The SEM micrographs of the products (Fig. 4 (a) and (b)) revealed that the surface morphology of both $Li_2Ni_8O_{10}$ and $LiMn_2O_4$ particles are quasi-spherical. However, the narrow distribution of the particles with homogeneous size distribution in $LiMn_2O_4$ reveals a pure particle formation. A heterogeneous morphology of $Li_2Ni_8O_{10}$ nanoparticles indicates an agglomerated graining structure. The calculated average grain size in both $Li_2Ni_8O_{10}$ and $LiMn_2O_4$ are about 18 to 32 nm.

Diffuse reflectance spectroscopy

DR spectra of $Li_2Ni_8O_{10}$ and $LiMn_2O_4$ nanoparticles were obtained at 200 and 1000 nm are shown in Fig. 5 (a and b). $Li_2Ni_8O_{10}$ and $LiMn_2O_4$ both show a sharp peak at around 310 nm.

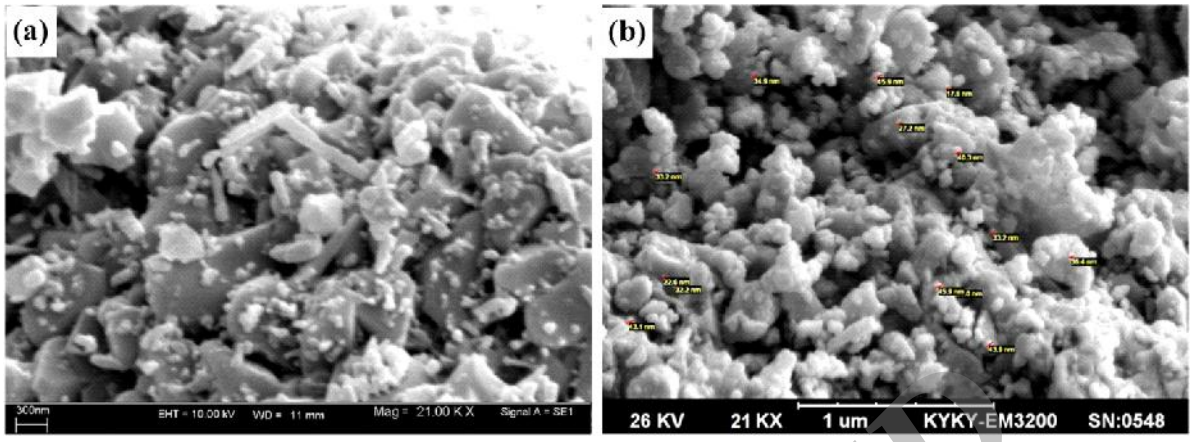

Fig. 4: SEM micrographs of (a) $Li_2Ni_8O_{10}$ and (b) $LiMn_2O_4$ nanoparticles.

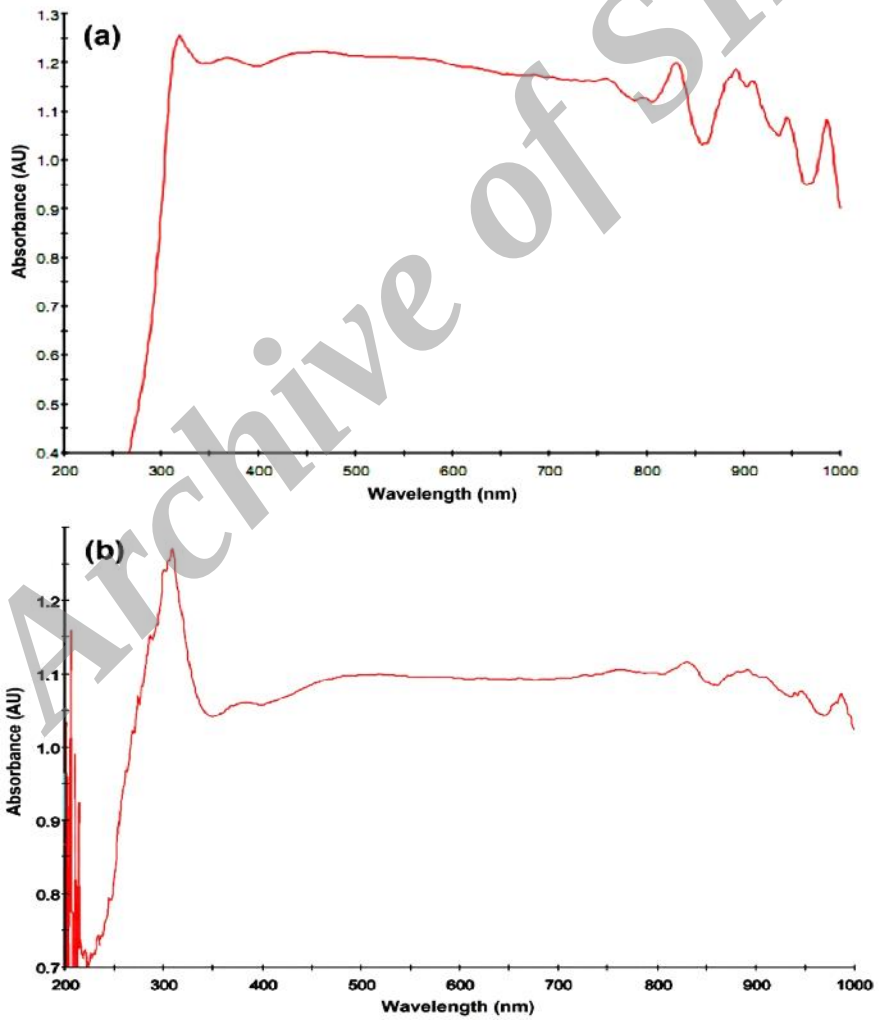

Fig. 5: DR spectra of (a) $Li_2Ni_8O_{10}$ and (b) $LiMn_2O_4$ nanoparticles.

The energy gap (E_g) is an important feature of semiconductors which determines their applications in optoelectronics [26–30]. A common way of extracting band gap from absorption spectra is to get the first derivative of absorbance with respect to photon energy and finding the maximum in the derivative spectra at the lower energy sides [31, 32]. The Tauc model (2) was used to determine the nature of the optical inter-band transition and value of the energy gap E_g,

$$(\alpha hv)^2 - A(hv - E_g) \qquad (2)$$

where α, A, hv and E_g are the absorption coefficient, edge width parameters independent of photon energy, energy of incident photon and band gap of the material, respectively. The band gap was obtained by extrapolating the straight portion of the graph on *hv* axis at $(\alpha hv)^2$ values (Fig. 6). The optical absorption curve results has been demonstrated that the band gap of $Li_2Ni_8O_{10}$ and $LiMn_2O_4$ are about 1.40 and 1.16 eV, respectively. Thus, the synthesized materials are semiconductor material and they can be used in photoelectric devices.

Photoluminescence spectroscopy

PL spectra of the $Li_2Ni_8O_{10}$ and $LiMn_2O_4$ nanoparticles are shown in Fig.7 (a and b). A broad and weak peak appears at around 400 nm in $LiMn_2O_4$ sample with a general broadening of the PL spectrum ranging from 350 to 500 nm. This indicates that the $LiMn_2O_4$ nanoparticles have a weak photoluminescence property due to forbidden spin of Mn^{2+} ($3d^5$). But, the $Li_2Ni_8O_{10}$ shows a slightly sharp peak at around 459 nm indicating intense photoluminescence property as compare to $LiMn_2O_4$ nanoparticles.

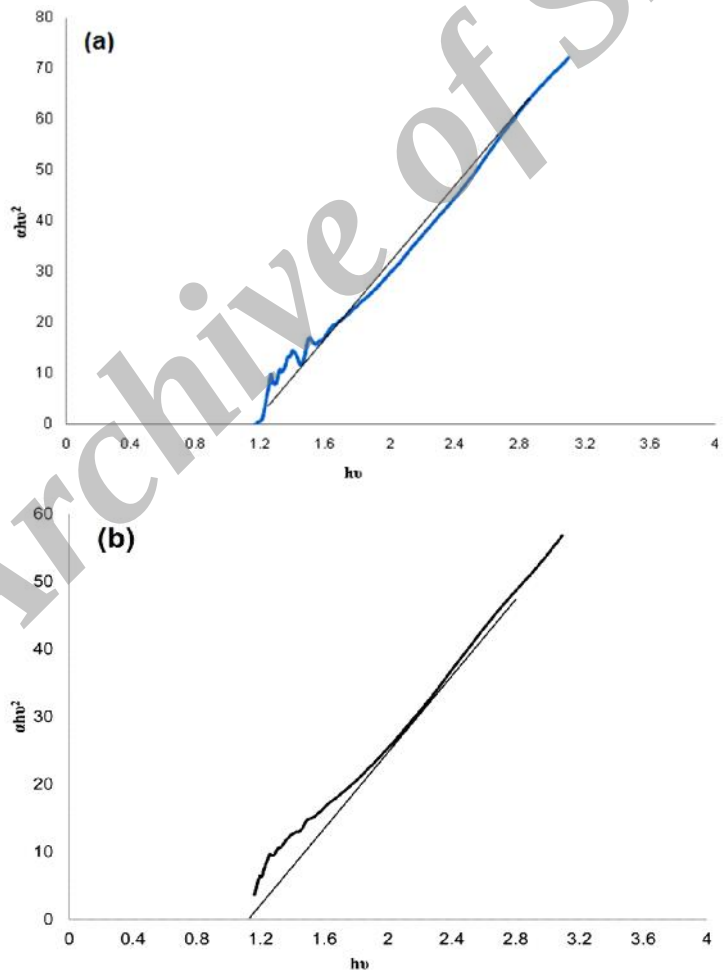

Fig. 6: The optical band gap of (a) $Li_2Ni_8O_{10}$ and (b) $LiMn_2O_4$ nanoparticles.

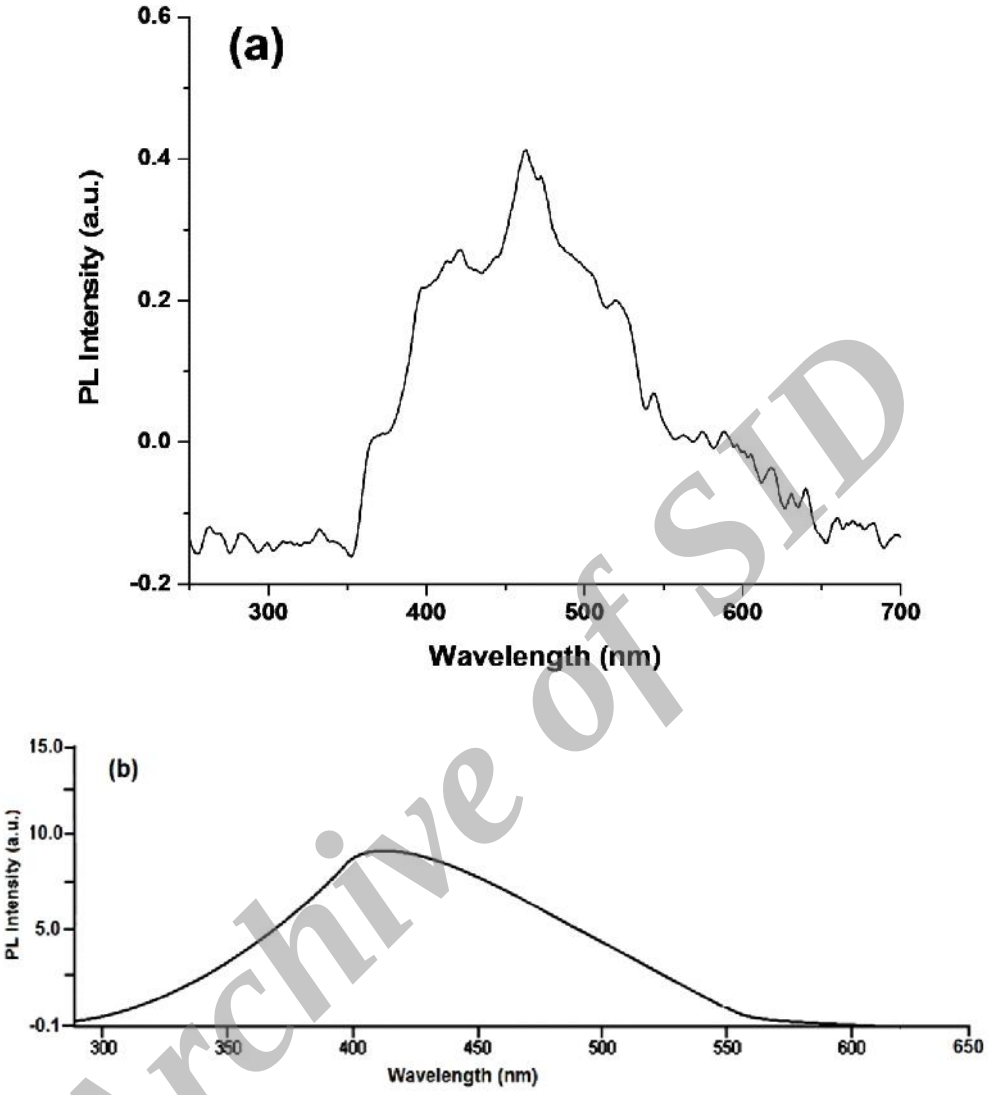

Fig. 7: PL spectra of (a) $Li_2Ni_8O_{10}$ and (b) $LiMn_2O_4$ nanoparticles.

Magnetic property of $LiMn_2O_4$ nanoparticles

Fig. 8 shows the measured hysteresis loops $LiMn_2O_4$ nanoparticles. Comparison of the hysteresis loops of the nanoparticles measured at room temperature with typical curves obtained from mixed magnetic systems shows a paramagnetic behavior of the products. From the results, it can observe that the $LiMn_2O_4$ nanoparticles are paramagnetic and magnetization parameter obtained at 0.4 emu/g in 8kOe applied field.

Color properties ($L^*.a^*.b^*$) of $LiMn_2O_4$ nanoparticles

The L*.a*.b*, or CIE Lab, color space (Fig. 9) is an international standard for color measurements, adopted by the Commission International d'Eclairage (CIE) in 1976. L* is the luminance or lightness component, which ranges from 0 to 100, and parameters a* (from green to red) and b* (from blue to yellow) are the two chromatic components, which range from -120 to +120 [33]. The L*.a*.b* color parameters of $LiMn_2O_4$ nanoparticles obtained in this study from reflectance spectroscopy are shown in Table 1.

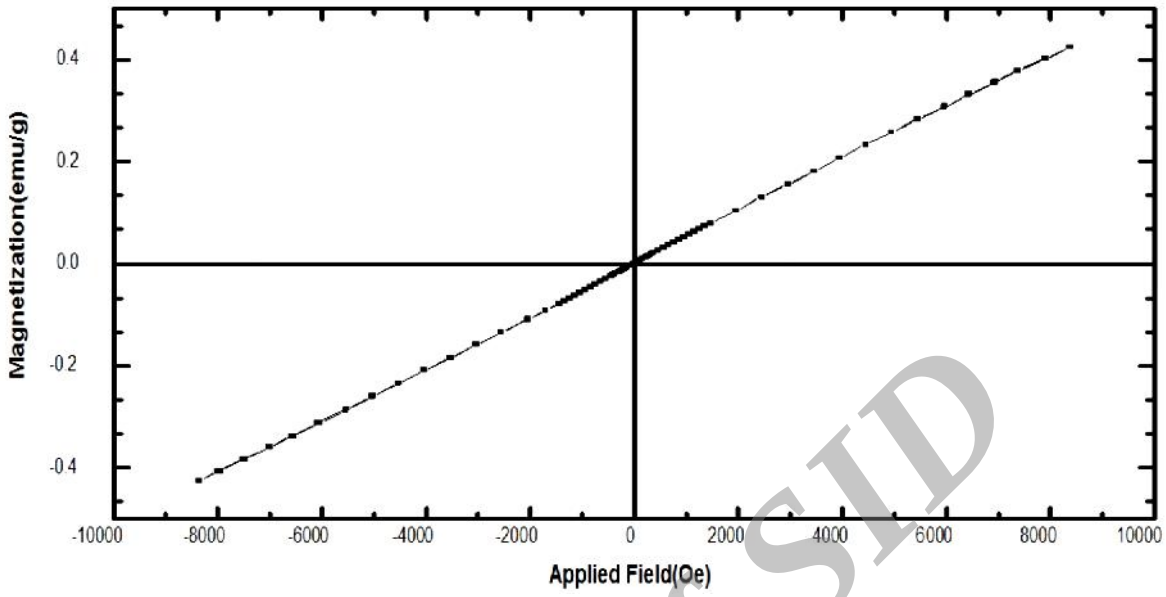

Fig. 8: VSM curve of the $LiMn_2O_4$ nanoparticles.

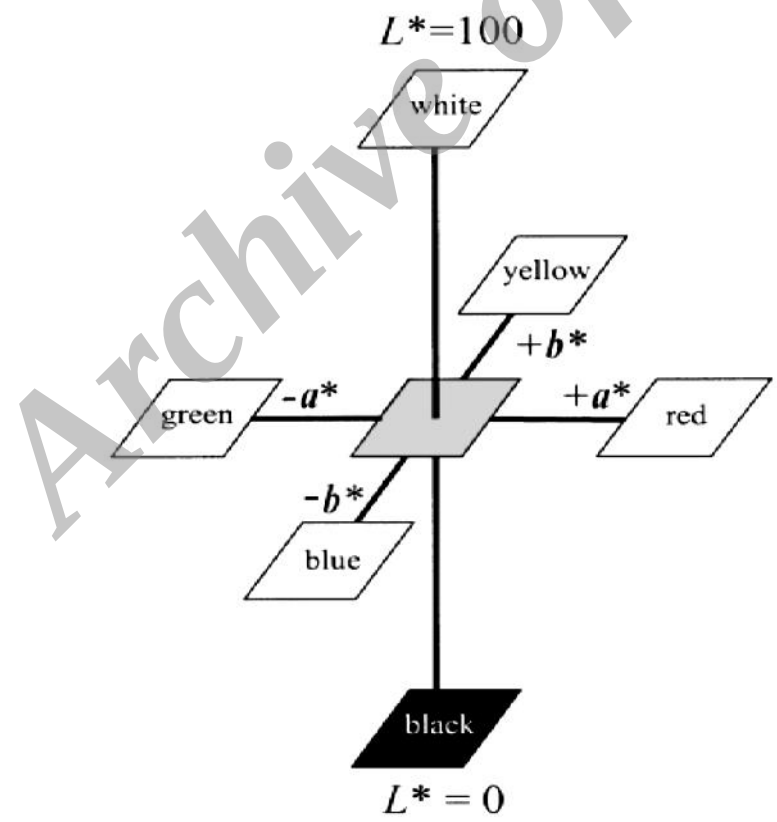

Fig. 9: Arrangement of color attributes in the CIE 1976 ($L^*.a^*.b^*$) color space.

Table: 1 Color ($L^*.a^*.b^*$) Parameters of $LiMn_2O_4$ nanoparticles.

Name	Illumination	L^*	a^*	b^*
$LiMn_2O_4$	D65	25.820	1.607	-1.143

CONCLUSION

Spinel $Li_2Ni_8O_{10}$ and $LiMn_2O_4$ nanoparticles were synthesized successfully by stearic acid gel process. $Li_2Ni_8O_{10}$ and $LiMn_2O_4$ were identified from their XRD patterns as a main crystalline phase with presence of minor impurities. SEM micrographs indicate the particle size ranging from 30 to 50 nm for $Li_2Ni_8O_{10}$ and $LiMn_2O_4$ nanoparticles. The band gap of $Li_2Ni_8O_{10}$ obtained at 1.40 eV and for $LiMn_2O_4$ at 1.16 eV. Therefore, the both synthesized nanoparticles can be used as semiconductor in photoelectric devices. Color parameters evaluated by colorimetric analysis of $LiMn_2O_4$ resulted characteristic values of L*=25.820, a*=1.607 and b*=-1.143.

ACKNOWLEDGEMENT

The authors wish to thank Iran Nanotechnology Initiative Council and Islamic Azad University (Mahabad and Naragh branch) for their support.

REFERENCES

[1] Guyomard D., Tarascon J. M., (1992), Li metal-free rechargeable $LiMn_2O_4$ carbon cells: their understanding and optimization. *J. Electrochem. Soc.* 139: 937–948.

[2] Wan C, Nuli Y, Zhuang J, Jiang Z., (2002), Synthesis of spinel $LiMn_2O_4$ using direct solid state reaction. *Mater. Lett*. 56: 357-363.

[3] Sahan H., Goktepe H., Patat S., Ulgen A., (2011), Improvement of the electrochemical performance of $LiMn_2O_4$ cathode active material by lithium borosilicate (LBS) surface coating for lithium-ion batteries. *J. Alloys Compd*. 509: 4235-424.

[4] Ahn D. S, Song M. Y., (2000), Variations of the electrochemical properties of $LiMn_2O_4$ with synthesis conditions. *J. Electrochem. Soc.* 147: 874-879.

[5] Huo J., Wei M., (2009), Characterization and magnetic properties of nanocrystalline nickel ferrite synthesized by hydrothermal method. *Mater. Lett.* 63: 1183-1184.

[6] Li X, Wang G., (2009), Low-temperature synthesis and growth of super paramagnetic $Zn_{0.5}Ni_{0.5}Fe_2O_4$ nanosized particles. *J. Magn. Magn. Mater*. 321: 1276-1279.

[7] Dai Z. F, Liu G. Y., Wang B. S., Guo D. W., Huang Z. L., Guo J. M., (2008), Solution combustion synthesis of $LiMn_2O_4$ powder by using glucose as fuel in acetate system. *J Funct. Mater.* 39: 254-256.

[8] Lee K. M, Choi H. J, Lee J. G., (2001), Combustion synthesis of spinel $LiMn_2O_4$ cathode materials for lithium secondary batteries. *J. Mater. Sci. Lett*. 20: 1309-1311.

[9] Yang W. S., Zhang G., Xie J.Y., Yang L. L., Liu Q. G., (1999), A combustion method to prepare spinel phase $LiMn_2O_4$ cathode materials for lithium-ion batteries, *J. Power Sources*. 81-82: 412-415.

[10] Passerini S., Coustier F., Giorgetti M., Smyrl W. H., (1999), Li–Mn–O aerogels. *Electrochem. Solid-State Lett*. 2: 483–485.

[11] Naghash A. R., Lee J. Y., (2000), Preparation of spinel lithium manganese oxide by aqueous co-precipitation. *J. Power Sources*. 85: 284–293.

[12] Xia Y.,Takeshige H., Noguchi H., Yoshio M., (1995), Studies on a Li–Mn-O spinel system (obtained by melt-impregnation) as a cathode for 4V lithium batteries. Part 1. Synthesis and electrochemical behaviour of $Li_xMn_2O_4$. *J. Power Sources*. 56: 61–67.

[13] Yang W., Liu Q., Qiu W., Lu S., Yang L., (1999), A citric acid method to prepare $LiMn_2O_4$ for lithium–ion batteries. *Solid State Ionics*. 121: 79–84

[14] Hon Y. M., Fung K. Z., Hon M. H., (2001), Synthesis and characterization of $Li_{1+\delta}Mn_{2-\delta}O_4$ powders prepared by citric acid gel process. *J. Eur. Ceram. Soc*. 21: 515–522.

[15] Tsumura T., Shimizu A., Inagaki M., (1997), Synthesis of $LiMn_2O_4$ spinel via tartrates. *J. Power Sources*. 3: 593–599.

[16] Pyun S. I., Choi Y. M., Jeng I. D., (1997), Effect of the lithium content on electrochemical lithium intercalation into amorphous and crystalline powdered $Li_{1+\delta}Mn_2O_4$ electrodes prepared by sol-gel method. *J. Power Sources*, 68: 593–599.

[17] Liu W., Farrington G. C., Chaput F., Dunn B., (1996), Synthesis and electrochemical studies of spinel phase $LiMn_2O_4$ cathode materials prepared by Pechini process. *J. Electrochem. Soc*. 143: 879–884.

[18] Ahn D. S., Song M. Y., (2000), Variations of the electrochemical properties of $LiMn_2O_4$ with synthesis conditions. *J. Electrochem. Soc.* 147: 874-879.

[19] Yang W. S., Zhang G, Xie J. Y., Yang L. L., Liu Q. G., (1999), A combustion method to prepare spinel phase $LiMn_2O_4$ cathode materials for lithium-ion batteries.W *J. Power Sources*. 82: 412-415.

[20] Gao Y., Dahn J. R., (1996), Synthesis and characterization of $Li_{1+x}Mn_{2-x}O_4$ for Li–ion battery applications. *J. Electrochem. Soc*. 143: 100–114

[21] Endres P., Fuchs B., Sack S. K., Brandt K., Becker G. F., Praas H. W., (1996), Influence of processing on the Li:Mn ratio in spinel phases of the system $Li_{1+x}Mn_{2-x}O_{4-\delta}$. *Solid State Ionics*. 89: 221–231.

[22] Enhessari M., (2013), Synthesis, characterisation and optical band gap of $Cr_{1.3}Fe_{0.7}O_3$ nanopigments. *Pigment and Resin Technol.* 42: 347-352.

[23] Hon Y. M., Lin S. P., Fung K. Z., Hon M. H., (2002), Synthesis and characterization of nano-$LiMn_2O_4$ powder

by tartaric acid gel process. *J. Europ. Ceramic Soc.* 22: 653–660.

[24] Tarascon J. M., Mckinnon W. R., Coowar F., Bowmer T. N., Amatucci G., Guyomard D., (1994), Synthesis condition and oxygen. *J. Electrochem. Soc*. 141: 1421-1427.

[25] Seyedahmadian M., Houshyarazar S., Amirshaghaghi A., (2013), Synthesis and Characterization of Nanosized of Spinel $LiMn_2O_4$ via Sol-gel and Freeze Drying Methods. *Bull. Korean Chem. Soc*. 34: No. 2.

[26] Zhou X., Chen M., Xiang M., Bai H., Guo J., (2013), Solid-state combustion synthesis of spinel $LiMn_2O_4$ using glucose as a fuel. *Ceramics Int.* 39: 4783–4789.

[27] Yang T., Bian J., Liang H., Sun J., Wang H., Liu W., Chang W., (2013), High quality p-type ZnO films grown by low pressure plasma-assisted MOCVD with N 2 O rf plasma doping source. *J. Mater. Process. Technol.* 204: 481–485.

[28] Bagnall D. M., Chen Y. F., Zhu Z., Yao T., Koyama M., Shen M. Y., Goto T., (1997), Optically pumped lasing of ZnO at room temperature. *Appl. Phys. Lett*. 70: 2230–2232.

[29] Aoki T., Hatanaka Y., Look D. C., (2000), ZnO diode fabricated by excimer-laser doping. *Appl. Phys. Lett.* 76: 3257–3259.

[30] Boemare C. T., Monteiro M. J., Soares J. G., Guilherme Alves E., (2001), Photoluminescence studies in ZnO samples. *Physica B*. 308: 985–988.

[31] Escobedo M. A., Sa´nchez M. E., Pal U., (2006), Use of diffuse reflectance spectroscopy for optical characterization of un-supported nanostructures, *Revista Mexicana*. 53: 18–22.

[32] Ouyang C., Deng H., Ye Z., Lei M., Chen L., (2006), Pulsed laser deposition prepared $LiMn_2O_4$ thin film. *Thin Solid Films.* 503: 268 – 271.

[33] Papadakis S. E., Abdul-Malek S., Kamdem R. E., Yam K. L., (2000), A versatile and inexpensive technique for measuring color of foods. *Food Technol.* 54: 48–51.

How to cite this article: (Vancouver style)

Nouri J., Khoshravesh T., Khanahmadzadeh S., Salehabadi A., Enhessari M., (2016), Synthesis, characterization and optical band gap of Lithium cathode materials: $Li_2Ni_8O_{10}$ and $LiMn_2O_4$ nanoparticles. *Int. J. Nano Dimens.* 7(1): 15-24.

DOI: 10.7508/ijnd.2016.01.002

URL: http://ijnd.ir/article_15298_2444.html